www.czasopisma.pan.pl PAN POLSKA AKADEMIA NAUK www.journals.pan.pl

Arch. Metall. Mater. **68** (2023), 3, 1127-1135

DOI: https://doi.org/10.24425/amm.2023.145484

T. GORYCZKA[1*], G. DERCZ[1]

EFFECT OF MILLING TIME ON CRYSTALLIZATION SEQUENCE AND MICROSTRUCTURE OF NiTi ALLOYS PRODUCED VIA HIGH-ENERGY BALL MILLING

A 20 gram batch weight of NiTi alloy, with a nominal equiatomic composition, was produced by mechanical alloying with milling times of 100, 120, and 140 hours. The differential scanning calorimetry was used to analyze the progress of the crystallization process. The X-ray diffraction examined the crystal structure of the alloy at individual crystallization stages. The observation of the powders microstructure and the chemical composition measurement were carried out using a scanning electron microscope equipped with an energy-dispersive detector. After the milling process, the alloy revealed an amorphous-nanocrystalline state. The course of the crystallization process was multi-stage and proceeded at a lower temperature than the pure amorphous state. The applied production parameters and the stage heat treatment allowed to obtain the alloy showing the reversible martensitic transformation with an enthalpy of almost 5 J/g.

Keywords: NiTi alloy; mechanical alloying; milling conditions; crystallization

1. Introduction

Many methods and techniques adapted from classical metallurgy are used for the NiTi alloy production. These are conventional casting methods, such as: vacuum induction melting (VIM), vacuum arc remelting (VAR), electron beam melting (EBM) [1-3], additive manufacturing techniques [4], or powder metallurgy [5-7]. In order to avoid the transition to the liquid phase, the production interest was directed to powder metallurgy. Hence, techniques such as conventional sintering (SC) [8], self-propagating high-temperature synthesis SHS) [9], hot isostatic pressing (HIP) [10], metal injection molding (MIM) [11] or spark plasma sintering (SPS) [12] were adopted for the shape memory alloys production. In this way, a bulk material can be produced using the diffusion of alloying elements in the solid state. Due to the potential of using the shape memory effect in composites, there has been research on producing the NiTi alloys in the form of powders with grain sizes of nano and/or micrometers.

For these purposes, milling in high-energy mills can be applied, which, in addition to milling particles, leads to the alloying elements diffusion, enabling their amorphization and/or mechanical alloying [10,13-15]. Similarly to all production methods, powder metallurgical techniques have advantages and disadvantages. An undoubted benefit is a possibility to start from individual alloying elements and obtaining an alloy in the form of a powder with grain sizes of a few nanometers to agglomerates measuring several hundred micrometers. The final structure, phase composition, and chemical composition are determined by various factors, such as: the mill type, container capacity, milling speed, batch weight, milling time, ball-to-powder weight ratio, protective atmosphere, etc. The milling time and speed are relatively easy to control and have the most significant impact on the alloy form. However, the high reactivity of titanium must be taken into account, and the production conditions should not lead to an increase in the container's temperature. In the case of the NiTi alloy, a too high speed may lead to an increase in temperature and thus create favorable conditions for oxidation. As a result, the thin titanium oxide layer forming on particles may completely block the diffusion process. The millingtime is the second parameter to control the process. Apart from grain fragmentation and amorphization, mechanical alloying can be achieved by the appropriate time. This property is essential for NiTi alloys due to the reversible martensitic transformation and the shape memory effects. The martensitic transformation does not occur in the amorphous state, so memory effects cannot be expected.

[1] UNIVERSITY OF SILESIA IN KATOWICE, INSTITUTE OF MATERIALS SCIENCE, 75 PUŁKU PIECHOTY 1A STR., 41-500 CHORZOW, POLAND

* Corresponding author: tomasz.goryczka@us.edu.pl

The paper attempts to describe: the mechanism of the NiTi alloy formation, the crystallization sequence of its phase components, and the formation of the intermetallic β phase, which undergoes the reversible martensitic transformation. The description was done qualitatively and quantitatively.

2. Materials and Methods

The NiTi alloy, with a nominal chemical composition of 50at.% Ti and Ni was prepared from commercial powders with a purity of 99.7% and an average particle size of 34 µm and 11 µm, respectively. The milling process was carried out in the high-energy Fritsch Pulverisette 7 premium line planetary-ball mill with the following parameters: milling speed 250 rpm; ball-to-powder weight ratio 10:1; ball size 10 mm; batch weight 20 g; milling time 100 h, 120 h, and 140 h; and an Ar protective-gas atmosphere.

The crystallization and the martensitic transformation were studied using the Mettler Toledo DSC 1 calorimeter. Before the measurements series, the calorimeter was calibrated using an indium standard. The characteristic temperatures of the phase transitions were determined from the intersection of the tangent line drawn to the side of the peak with the baseline. The thermal peaks were detected automatically as a deviation from the baseline, applying the software provided by Mettler Toledo. The course of the baseline was also determined during the calibration.

First, the thermograms were measured up to 610°C with a heat rate of 20°/min. The crystallization effect appeared in the thermal range from 355°C and 590°C. However, several thermal peaks were observed. In order to determine the crystallization sequence, the samples of about 40-50 mg were *in-situ* heated to the temperatures marked with the "T" index in Fig. 1. Next, the samples were held for 5 minutes and cooled down, with the highest speed, to –120°C. Finally, the two cycles were measured in the temperature range from –120°C to 120°C at a rate of 10 deg/min. The samples were then subjected to microscopic observations and structural examinations.

The microstructure observation was carried out using the JEOL JSM 4680 (JEOL, Ltd., Tokyo, Japan) scanning electron microscope (SEM) equipped with an X-ray energy dispersive spectrometer (EDS). The accelerating voltage was 20 kV.

The phase identification was performed from the X-ray diffraction patterns measured using the Phillips X-ray X'Pert ((PANalytical, Almelo, The Netherlands)) diffractometer with copper radiation ($CuK_{1\ and\ 2}$). All the measurements were done at room temperature in an angular 2θ range: 10-140°, in a step-scan mode with the step of 0.04°. The time of measurement was adjusted to receive appropriate counting statistics. The ICDD-PDF-4+ (International Centre for Diffraction Data) database was used for the phase identification. In order to determine the crystallographic parameters and carry out the phase quantitative analysis, the X-ray diffraction patterns were subjected to the Rietveld refinement [16]. The crystallographic data sets taken from the ICDD PDF 4+ database were applied to build the starting model of the crystal lattice or the amorphous-nanocrystalline phase. For the solid solution: nickel-based and titanium-based, the data from card no. ICDD PDF 00-004-0850, and ICDD PDF 00-044-1294 were used, respectively. For convenience, the transformable phases were modeled as follows: the data from card no. ICDD PDF 03-065-0917 for the B2 parent phase, the card no. ICDD PDF 04-011-1996 for the R-phase, and the card no ICDD PDF 03-065-0365 for the B19' monoclinic martensite. The data from the cards: ICDD PDF 00-051-1169 and ICDD PDF 00-018-0898 were applied for non-transformable equilibrium phases Ni_3Ti and Ti_2Ni, respectively. The calculations were done using the LHPM computer program (version 4.2. Lucas Heights Research Laboratories ANSTO, Sydney, Australia).

3. Results and discussion

3.1. Multi-stage crystallization

The crystallization of the 20-gram samples and the 10-gram ones was completely different. After 100 hours of milling, the 10 g batch was a powder with an average crystallite size of about a few nanometers. In this case, the crystallization was carried out as a single stage in the thermal range from 530°C to 539°C [17]. Contrary, in the 20 g batch, the crystallization possessed a multi-stage character, even when the milling time was extended to 140 hours [18]. The temperatures of individual crystallization peaks were marked with the "P" index (Fig. 1). Moreover, the crystallization in this temperature range was not only a process with endothermic demand. From 350°C to 610°C, an increase in the baseline was observed, indicating the additional energy need for another endothermic process.

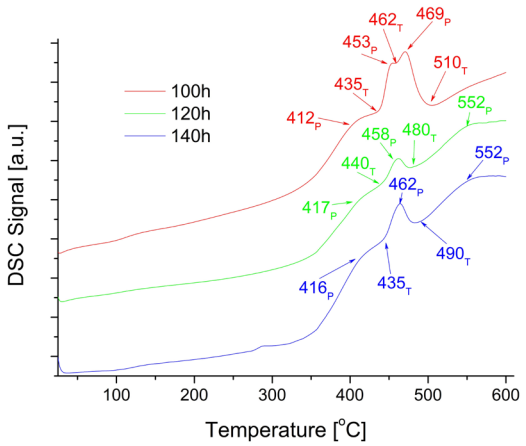

Fig. 1. Set of DSC heating curves measured for samples milled 100 h, 120 h, and 140 h

The X-ray diffraction patterns of the thermally treated samples (at intermediate temperatures marked as "T" – Fig. 1) were measured to identify the sequence of phases undergoing

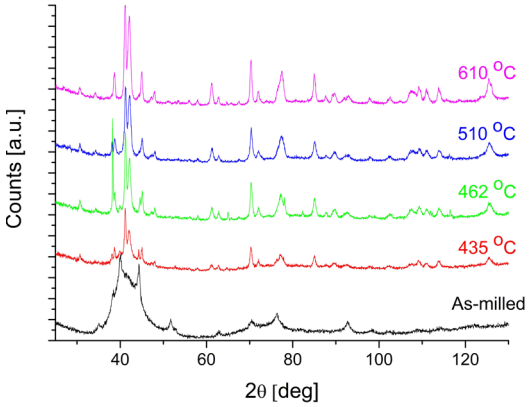

Fig. 2. Set of the X-ray diffraction patterns measured for powders mixed 100 h and additionally annealed at various temperatures for 5 minutes

crystallization and determine their quantitative contribution. An example of the measured X-ray diffraction patterns for the powders mixed for 100 hours is shown in Fig. 2.

After the phase identification, the theoretical diffraction patterns were calculated using the crystallographic data and fitted to the measured ones via the Rietveld method [16]. The reliability factors that characterize the quality of refinements, such as R_p, R_w, and R_{exp}, were at most 6, 7, and 4.5%, respectively. The examples of the Rietveld refinement done for the X-ray diffraction patterns measured for the milled 120 hours and annealed powders are shown in Fig. 3. Based on the calculations, their contents [wt.%] were determined. The results are summarized in TABLE 1.

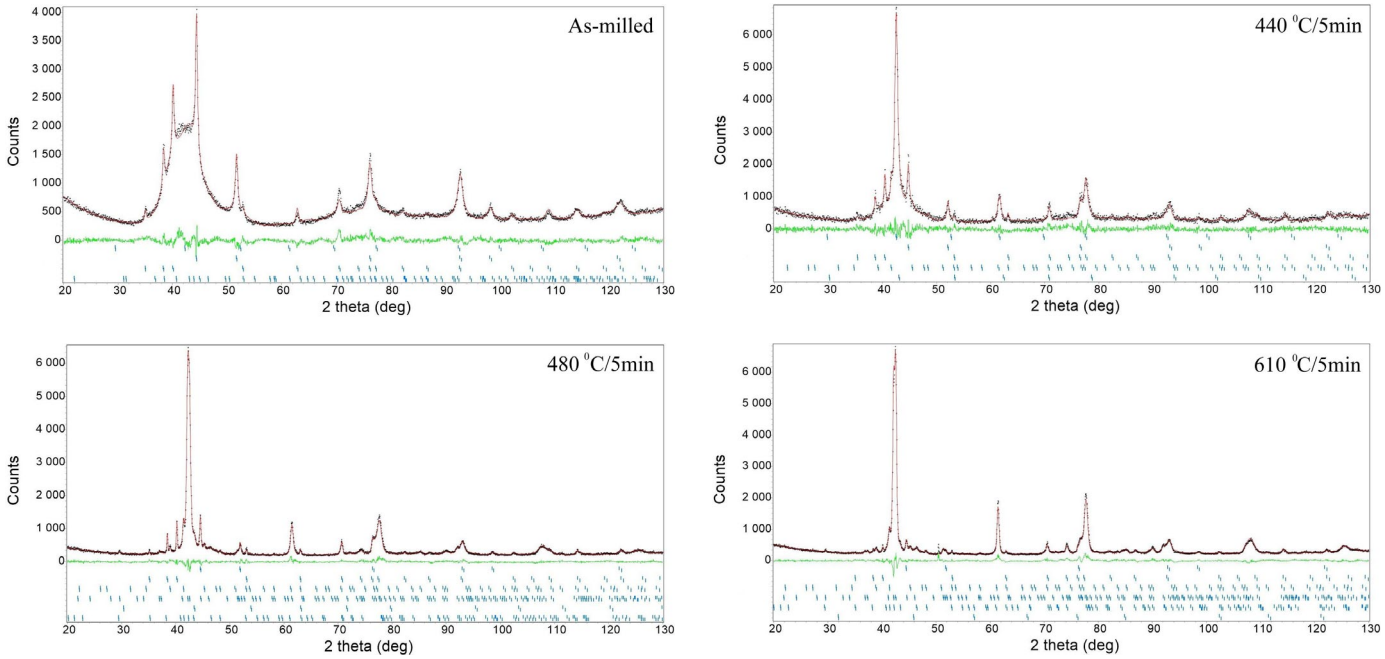

Fig. 3. Results of the Rietveld refinement carried out for the X-ray diffraction pattern measured for powders milled 120 hours and annealed for 5 minutes at various temperatures

TABLE 1

Phase composition, its weight percentage in dependence on milling time and thermal treatment conditions

Milling time [h]	Treatment conditions	Weight percentage [%]									
		Amorphous - nanocrystalline mixture	Non-transformable phases				Transformable phases			Sum of transformable phases	Total
			Solid solutions		Ni_3Ti	Ti_2Ni	B2	R-phase	B19'		
			Ni-based	Ti-based							
100	As-milled	75.2	1.4	0.3	—	—	23.1	—	—	23.1	100
	435°C/5min	9.9	0.1	11.8	8.1	18.5	42.7	—	8.9	51.6	100
	462°C/5min	0.1	—	0.2	—	8.9	71.4	—	19.5	90.8	100
	510°C/5min	—	—	—	—	4.4	88.6	—	7.0	95.6	100
	610°C/5min	—	—	—	—	44.7	1.1	—	54.2	55.3	100
120	As-milled	84.0	3.3	0.6	—	—	12.1	—	—	12.1	100
	440°C/5min	3.8	3.7	38.2	—	32.9	21.4	—	—	21.4	100
	480°C/5min	0.1	1.1	1.5	2.3	13.1	81.9	—	—	81.9	100
	610°C/5min	—	0.3	0.5	2.4	17.8	—	79.0	—	79.0	100
140	As-milled	80.3	3.6	0.3	—	—	15.8	—	—	15.8	100
	435°C/5min	0.7	0.5	14.9	—	81.1	2.8	—	—	2.8	100
	490°C/5min	—	—	0.6	4.2	1.2	92.2	—	1.8	94.1	100
	610°C/5min	—	—	0.1	2.4	18.5	—	75.1	3.9	79.0	100

3.2. Evolution of the amorphous-nanocrystalline state of powder

First of all, in the as-milled samples, the share of the amorphous-nanocrystalline mixture was relatively high, and after 100 hours of milling it was 75%. This share increased to 85% after 120 hours of milling, whereas after 140 hours it decreased to 80%. This fact can be explained as follows. On the one hand, the balls collision and the milling time extended, thus it provided more energy and enabled the alloy amorphization. On the other hand, some part of this energy was converted into thermal energy, increasing the charge temperature. Despite the milling breaks, the powder/balls collisions inside the jar could raise the local temperature even to several hundred degrees. This fact is known and widely described especially for the materials produced via the high-energy ball milling [19]. Vemula et al. showed that for the NiTi alloy, the jar's temperature could reach even 200 degrees [20]. In general, the batch stayed at the elevated temperatures by extending the milling time. Consequently, it led to the dynamic recrystallization and the growth of the average size of crystallites. As a result, extending the milling time to 140 h caused a decrease in the percentage of the amorphous-nanocrystalline mixture to 80%, when compared to 120 h. In return, the percentage of the other alloy components increased.

Annealing the batches milled for 100 h, and 140 h at 435°C for 5 minutes appeared to be a sufficient procedure to crystallize the alloy components. With the batch milled for 120 h the crystallization temperature was 440°C. After that, the amount of the amorphous-nanocrystalline mixture decreased to 2% and 3% for 100 h and 120 h, respectively. In the sample milled for 140 h and annealed at 435°C, its amount decreased to 0.7%. An increase of the annealing temperature to 462°C (100 h) or 480°C (120 h) resulted in a further decrease in the share of the amorphous-nanocrystalline mixture, reaching the fractions of a percent. The annealing conditions at the temperatures above 480°C led to its disappearance.

3.3. Formation of the no-transformable equilibrium phases devoid of the martensitic transformation

Despite the relatively long milling time of 100-140 hours, the present components of the alloy were solid solutions based on nickel and titanium. As the milling time increased, the percentage of the nickel-based solid solution rose from 1.4% to 3.6% for 140 hours of milling. Titanium did the opposite. Regardless of the length of milling time, the Ti percentage was only 0.3% to 0.6%. The situation changed after the annealing procedure. After the first thermal peak, the percentage of the solution increased from 1.4% (100 h) to over 3% (120 h and 140 h). Further annealing stages led to a gradual reduction of Ni share. Finally, at the temperatures of 462°C (100 h), 480°C (120 h), and 435°C (140 h), only the fractional Ni shares were found. The titanium-based solid solution showed a similar tendency. The first stage of annealing caused a significant increase in the Ti share , up to 16% (100 h), 38% (120 h), or almost 15% in the 140 h milled batch. Similarly to the solid solution of nickel, as the annealing temperature was increased, the Ti percentage decreased to the fractions of a percent at the temperature ending the crystallization process. This situation can be explained as follows. Under the equilibrium conditions described in the Ni-Ti phase equilibrium system, the range of nickel solubility in titanium was limited to about 1 at.% at the eutectoid transformation temperature of 765°C [21]. As the temperature lowered, this range decreased. On the contrary, titanium in nickel could dissolve up to about 10at.% at the 1304°C – eutectic transformation temperature. Also, in this case, as the temperature was lowered to room temperature, the solubility decreased to a few %. However, during the high-energy ball milling, the phase equilibrium conditions get disturbed so that the solubility ranges may differ from the equilibrium one.

The presence of the solid solutions was also confirmed by the SEM observations and the measurements of the distribution of elements maps and the chemical composition determination. For example, Fig. 4 shows the result for a batch milled for 100 h and heated at 435°C for 5 minutes.

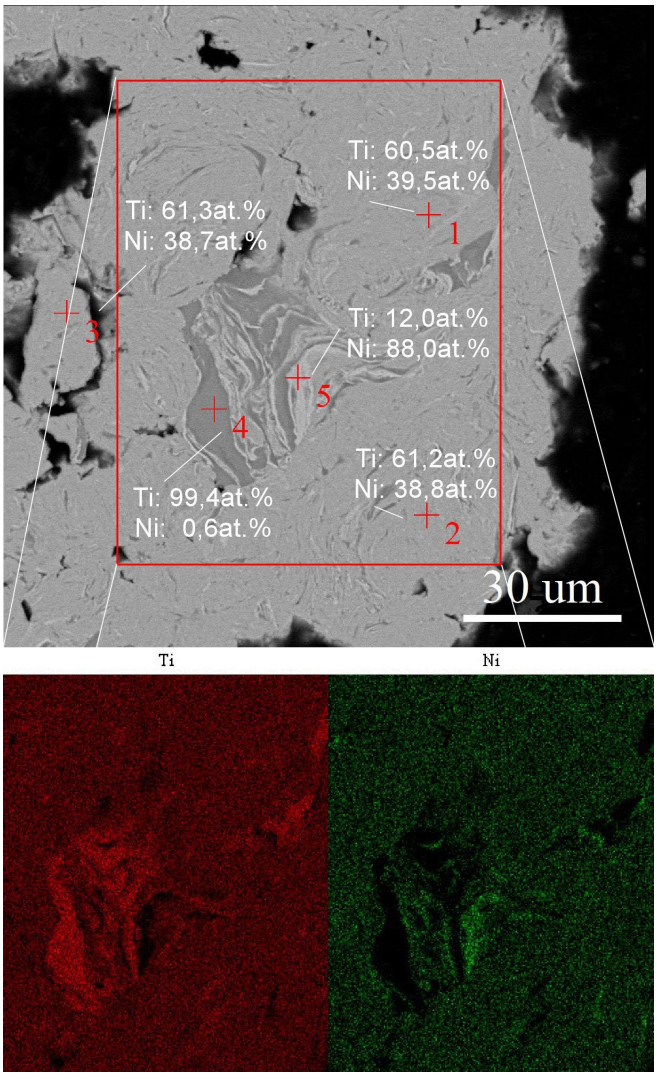

Fig. 4. SEM-BS image, element distribution map and determined chemical composition for batch milled 140 h and annealed at 490°C for 5 minutes

The microscopic image observed in backscattered electrons revealed a contrast from the chemical composition variation. Due to the conditions of electron scattering, the darker fields were characteristic for the increased presence of titanium and brighter ones for the increased amount of nickel. The maps of the distribution of elements confirmed that idea. In point „5" area, the high nickel content was clearly visible. The measured chemical composition: 12.0at.%Ti and 88at.%Ni confirmed that it was the nickel-based solid solution grain. In turn, the measurement at point „4" – the area enriched in titanium showed 99.4at.% Ti and 0.6at.% Ni. – proving the presence of the titanium-based solid solution. A gray tint characterized the remaining parts of the grain. The element distribution maps showed that these were areas evenly occupied by titanium and nickel. However, the measured chemical composition of the points marked as 1-3 showed the Ti presence at about 60.5-61.3 at.% and the share of nickel was at 39.5-38.7 at.%. This fact confirmed the presence of the equilibrium phase not undergoing the martensitic transformation – Ti_2Ni. Considering only the temperature range from the crystallization beginning – 355°C to its completion – 591°C, the weight percentage of the Ti_2Ni phase was the highest after the first stages of annealing and amounted to 19%, 33%, and 81%, respectively, for the samples milled 100 hours and 435°C/5 min; 120 hours and 440°C/5 min and 140 hours and 435°C/5 min respectively.

After annealing at the temperatures above 480°C and 490°C, the samples ground for 120 and 140 hours, respectively, caused the crystallization of the non-transformable Ni_3Ti phase. Its weight percentage did not exceed 2.4% and 4.2%, respectively. Its presence was confirmed by the chemical composition analysis and the distribution elements maps shown in Fig. 5. The chemical composition measured in the example area with higher contrast (point 4) revealed the Ni content above 70at.%, which is characteristic for this phase. The Ni_3Ti phase absence was stated in the as-milled state. Hence, its appearance may result from the intermetallic transformable β phase decay described by the conditions defined in the phase equilibrium system. Noteworthy is the fact that the chemical composition of the remaining areas was close to the equiatomic one – confirming the presence of the β transformable phase (points 1-3 in Fig. 5). In this case, the weight percentages indicated a content of almost 92%, and it consisted at room temperature mainly of the B2 phase and a small amount of the B19' martensite (TABLE 1).

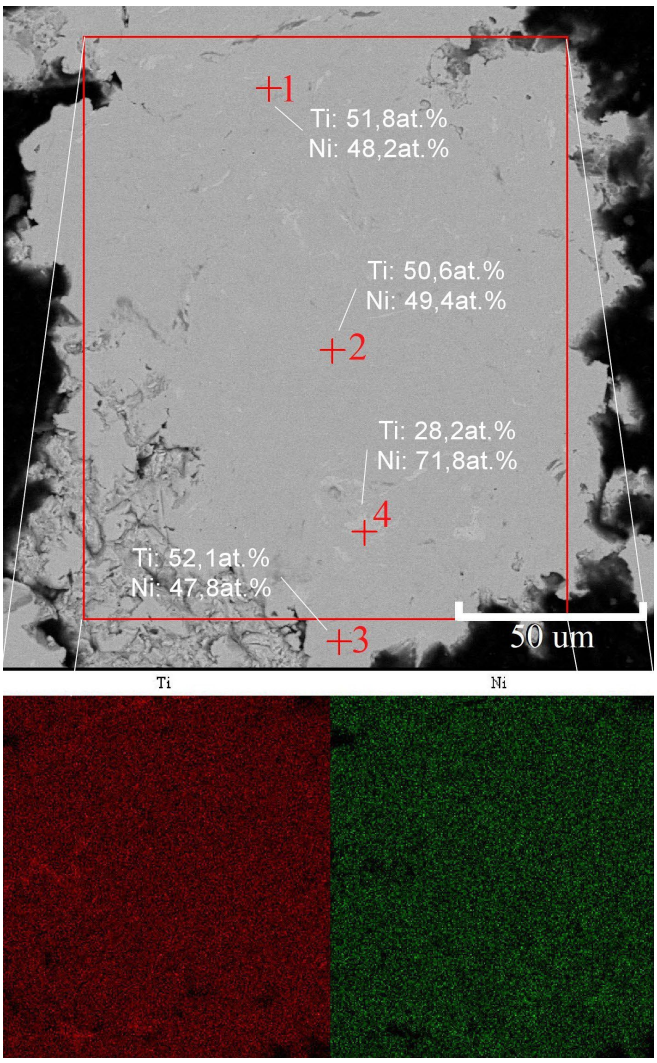

Fig. 5. SEM-BS image, element distribution map and determined chemical composition for batch milled 140 h and annealed at 490°C for 5 minutes

3.4. Formation of the β intermetallic equilibrium phase undergoing the martensitic transformation

According to the Ni-Ti equilibrium phase system, in an alloy with a chemical composition close to equilibrium, an intermetallic β phase appears in a temperature range from 630°C to about 1300°C. It undergoes the reversible martensitic transformation only in the crystalline state. As the temperature increases, the β phase concentration range extends to 1118°C and ranges from 49.5at.% to almost 57at.%. Below the eutectoid temperature (630°C), the β phase exists only at the equiatomic concentration. Practically, a vertical line up to room temperature is formed, separating the areas of the Ni_3Ti and Ti_2Ni equilibrium phases.

During milling, the phase equilibrium is disturbed. Hence a more comprehensive range of β phase concentrations is observed at room temperature. The martensitic transformation occurs between the high-temperature B2 parent phase and the monoclinic B19' martensite. In exceptional cases, e.g., with an increased nickel content, non-equilibrium Ni_4Ti_3 precipitates are formed, which cause a change in the transformation sequence by introducing additional internal stresses. Then, the one-stage B2 ↔ B19' sequence is changed to the two-stage B2 ↔ R ↔ B19' through the intermediate R-phase. The analyzed diffraction patterns (measured at room temperature) showed that the weight percentage of the β phases in the as-milled alloy was 23%, 12%, and almost 16% for 100, 120, and 140 hours, respectively. The crystal structure of the β phase took the form of B2. It means that the martensitic transformation occurs in the temperature region below room temperature. However, annealing at a temperature

above the first crystallization peak increases the amount of the β phase. For example, such a relationship is shown in Fig. 6 for 100 and 140 hours of milling as the sum of the weight percentage (marked with blue triangles). The quantitative characteristics for batch milled for 120 hours were very similar to the samples milled for 140 hours. In general, the amount of transformable β phase increased as the alloy passed through the second crystallization peak. It reached 84-95%, depending on the milling time. However, for the batch ground 100 hours and annealed at 435°C, the β phase consisted of 43% of the B2 phase and almost 9% of the B19' martensite (TABLE 1, Fig. 6). Annealing at 462°C almost doubled the parent phase B2 and the martensite B19 percentage (Fig. 6a). Increasing the annealing temperature to 510°C increased the amount of the parent phase to almost 89%. At the same time, the share of the Ti_2Ni phase decreased to 4%.

In contrast, annealing at 610°C (temperature above the crystallization end) provided conditions close to the thermodynamic equilibrium. Hence, the Ti_2Ni percentage increased to almost 45%. The transformable phase comprised 54% of the B19' martensite and 1% of the B2parent phase. No R-phase was found for this alloy. It means, that the phase transformation takes place only between the B2 parent phase and the B19' martensite.

The results obtained for the alloy milled for 120 hours were close to those of the alloy milled for 140 hours (TABLE 1). Thus, only the 140 h batch is discussed. After annealing, at 490°C (second crystallization peak), the percentage of the β phase rose to 94%. This transformable phase comprised the B2 parent phase (92%) and the B19' martensite (almost 2%). Moreover, the annealing conditions caused the β intermetallic phase to decay into Ti_2Ni (1.2%) and Ni_3Ti (4.2%) (Fig. 6b). The decay effect of the β phase was continuously observed after annealing at 610°C (after the crystallization end). The weight percentage of the Ti_2Ni phase increased to 18.5% with a certain amount of the Ni_3Ti phase (2.4%).

The almost wholly transformable β phase comprised the R-phase – 75% and almost 4% of the B19' martensite. It means that the extension of the milling time to 140 hours was a reason for the change of the martensitic transformation course with the R-phase.

3.5. Reversible martensitic transformation in the crystallization temperature range

The measurements, done using a differential scanning calorimeter, are supplemented and consistent with the obtained results and calculations. The measured thermograms are shown in Fig. 7. The characteristic temperatures of the martensitic transformation: M_s, M_f, A_s, A_f, and enthalpy were determined and presented in Figures 8 and 9, respectively. A comparison of the temperature ranges of thermal peaks showed that increasing the milling time to 140 hours shifted the temperature range the reversible martensitic transformation into the area of higher temperatures (Fig. 7). This phenomenon may result in the titanium diffusion from the untransformed equilibrium phases to the transformable β phase.

The course of the heating and cooling curves showed that the reversible martensitic transformation is one stage for the alloy milled for 100 hours and annealed at temperatures of 435°C-510°C and the alloy milled for 140 hours after the temperature of 435°C. There was one thermal peak on both the heating and cooling curves, respectively, and these two peaks broadened. This fact is known from the literature regarding the results from the heterogeneity of the chemical composition of the β phase. The previously described X-ray phase analysis showed that, at room temperature, the β phase consisted only of the B2 parent phase and the B19' martensite. Hence, this transformation was reversible and single-stage with the sequence B2 ↔ B19'. Increasing the annealing temperature in the ground alloy for 100 hours to 610°C led to its complete crystallization and changed the transformation nature from one stage to two stages, which was proved by the two visible overlapping thermal peaks.

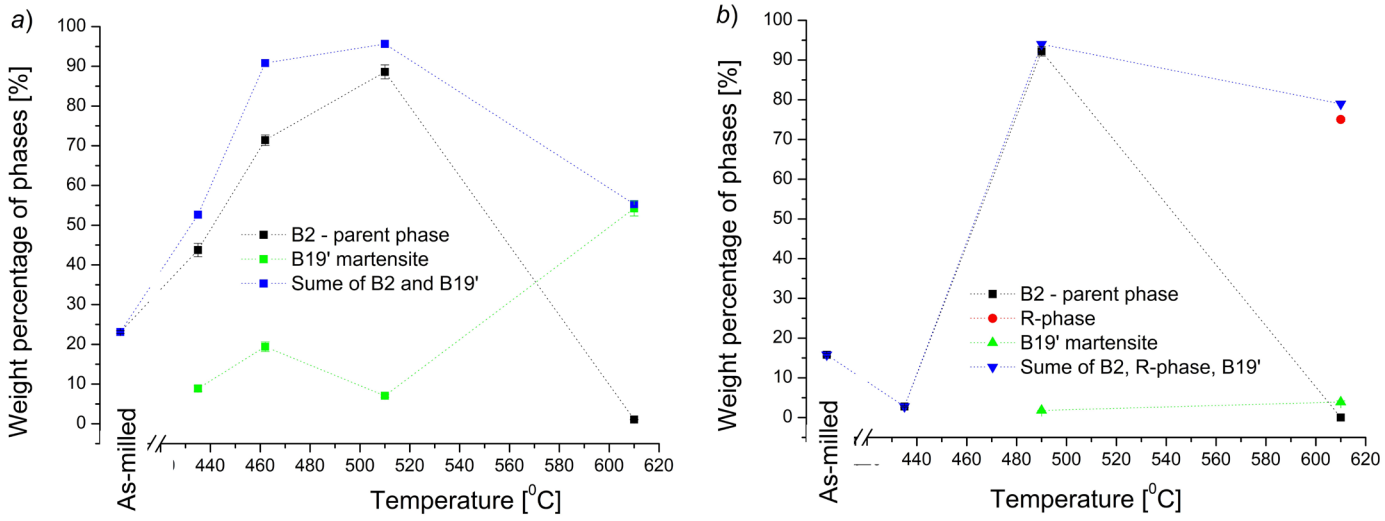

Fig. 6. Total weight share of transformable phase β with separation into phases involved in martensitic transformation for batch milled for 100 h (a) and 140 h (b)

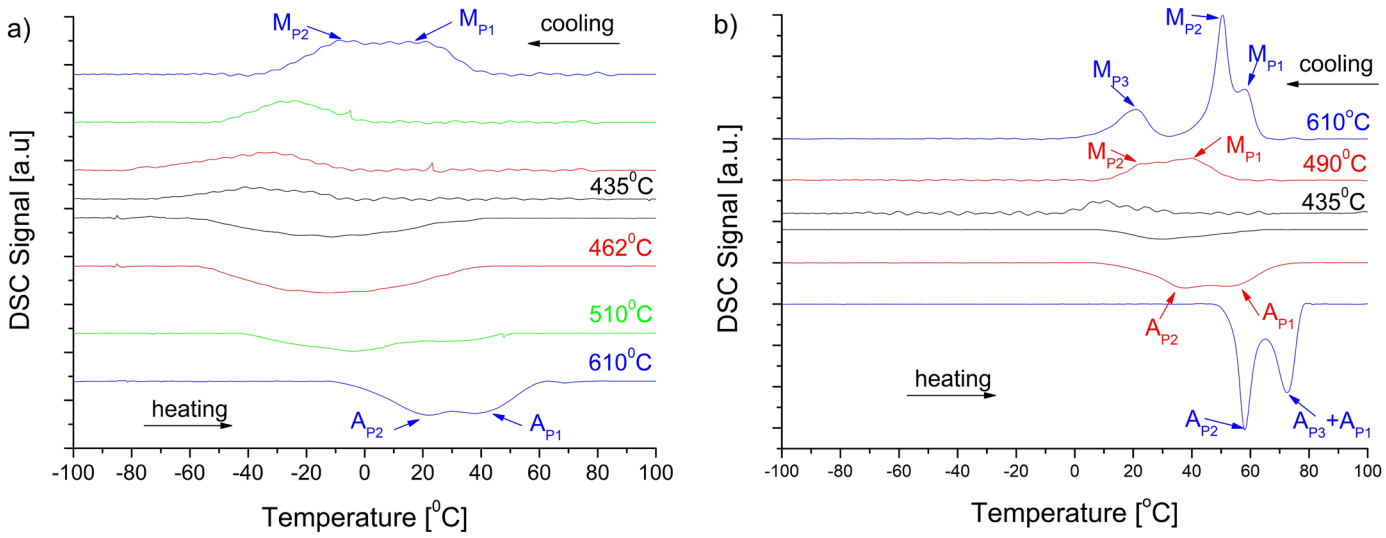

Fig. 7. Set of thermograms measured for samples annealed at temperatures after individual stages of crystallization process for the alloy ground for 100 (a) and 140 hours (b)

The determined differences between the peak temperatures of the corresponding transformation stages ($M_{P1} - A_{p1}$ = 20°C and $M_{P2} - A_{p2}$ = 28°C – blue color in Fig. 7a) showed that they were characteristic for the single-stage transformation with the B2 ↔ B19' sequence.

Such behavior is known from the literature [e.g.: 22] and results from the existence of areas of the transformable phase β with different nickel content. The higher nickel content shifts the transformation to lower temperatures. According to work [23] an increase in the titanium content by 0.1at.% (nickel loss) moves the characteristic temperatures by about 10 degrees to the area of higher temperatures. The calculated difference between M_{P1} and M_{P2} and, similarly, between A_{P1} and A_{P2} is about 20 degrees. Hence, it can be concluded that these areas differ by about 0.2at.% on average in the concentration of alloying elements. A similar two-stage martensitic transformation was demonstrated by the 140 hours milled alloy, additionally annealed at 490°C. Increasing the annealing temperature to 610°C completely changed the transformation behavior. The three thermal peaks on the DSC curve measured during cooling appeared and were marked as M_{P1}, M_{P2}, and M_{P3} (Fig. 7a – blue marks). For the reverse transformation, the two peaks were marked as A_{P2} and A_{P3}+ A_{P1}, respectively.The phase composition analysis showed that the transformed β phase consisted of the R-phase and the B19' martensite. It is well known that the difference in peak temperatures associated with the reversible transformation of the R-phase itself is from 7 to 10 degrees.

Furthermore, considering the previously discussed differences in the thermal peak of the B2 ↔ B19 transformation, it can be concluded that two independent martensitic transformations occured in this alloy: B2 ↔ B19' and B2 ↔ R ↔ B19' [24,25].

This fact may also be due to the volumes differing in chemical composition by only fractions of a percent [22]. One of the volumes was associated with the one-step transformation B2 ↔ B19' correlated with the forward transformation – peak M_{P1} and the reverse transformation – A_{P1}. The difference between the peaks temperature was about 17 degrees, and was characteristic for the B2 ↔ B19' transformation [7,24,25]. The second volume with the higher nickel content may be associated with the two-step transformation occurring during cooling and it composed of B2 → R (M_{P2}) and R → B19' (M_{P3}) [26].

The reverse martensitic transition proceeded from B19' to the R-phase (peak designated as A_{P2}). Then the R-phase transformed to the B2 parent phase (A_{P3} peak overlapped A_{P1}one). At the same range of temperatures, the volume with increased titanium content, still in the martensitic phase, was transformed directly into the B2 parent phase. Hence the second reverse transformation had the sequence B19' → B2. The additional proof of such an explanation may come from analyzing the enthalpy determined for the forward and reverse martensitic transformation.

In general, total enthalpy is a sum of transformation components comparable to those determined from reverse transformation [26]. Going into detail, the determined enthalpy associated with the R → B19' transformation (peak M_{P2}) is 2.43 J/g, while its equivalent in the reverse transformation B19' → R (peak A_{P2}) is 2.49 J/g. The sum of the enthalpies of transformations associated with the thermal peaks M_{P1} (0.75 J/g) + M_{P3} (1.24 J/g) is 1.99 J/g, and is comparable to the enthalpy associated with the overlapping transformations R → B2 (A_{P3} – 1.21 J/g) and B19' → B2 (A_{P1} – 0.84 J/g), and is 2.05 J/g [26].

In our study the characteristic temperatures for the forward and reverse martensitic transformations were determined from the intersection of the tangent to the side of the thermal peak with the baseline. The results are shown in Fig. 8. The characteristics showed that the values of the characteristic temperatures increased as the annealing temperature rose. However, they had a different course due to the single- or multi-stage nature of the transformations. In the 100 h milled alloy, in which the transformation occurred in one step between B2 and B19', the temperature range of the martensitic transformation (calculated as the difference between the M_f and A_f) decreased with the increase

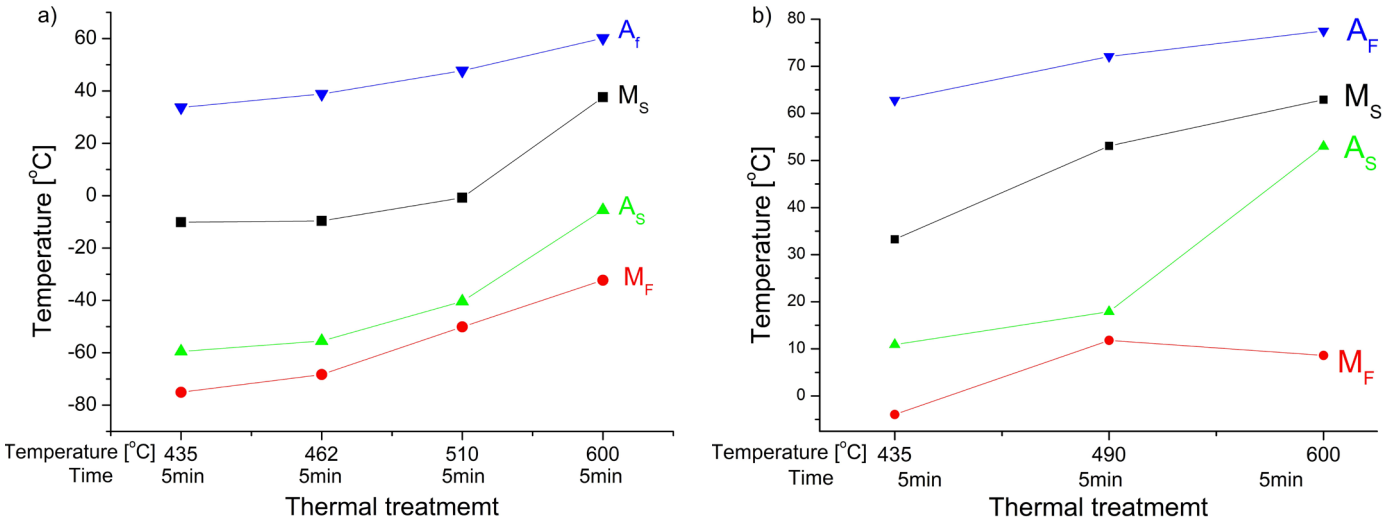

Fig. 8. Dependence of the characteristic temperatures of the martensitic transformation on the annealing temperatures related to the stages of the crystallization process for the ground alloy 100 h (a) and 140 (b)

of the annealing temperature. In addition, the thermal peaks width determined from the decrease in the temperatures of the transformation beginning and its end ($M_s - M_f$ and $A_s - A_f$). These effects resulted from the improvement of the homogeneity of the chemical composition. A similar characteristic was shown by the characteristic temperatures of the martensitic transformation depending on the annealing temperature determined for the 140 h ground alloy. However, the appearance of a two-step (after annealing at 490°C) and a two-stage transformation, involving the R-phase (after annealing at 610°C), caused a shift in the A_f and M_f temperatures. As a result, the temperature range expanded. The narrowing between the temperatures of A_s and A_f evidenced the progressing homogeneity of the chemical composition.

Equally important, apart from the characteristic temperatures, is the enthalpy for the martensitic transformation. It gives information about the ability to perform the shape memory phenomenon. This parameter is mainly related to the transformable β phase amount: the higher the content of the β phase, the higher value of the transformation enthalpy. The content of the transformable phase increased as the crystallization progressed (TABLE 1). Such a trend was reflected in the transformation enthalpy increase in the annealed samples (Fig. 9). Consequently, regardless of the milling time, the highest enthalpy value was obtained afterannealing at 610°C. Also, in this case, extending the milling time to 140 hours increased the enthalpy of transformation in the batch milled for 100 hours (Fig. 9).

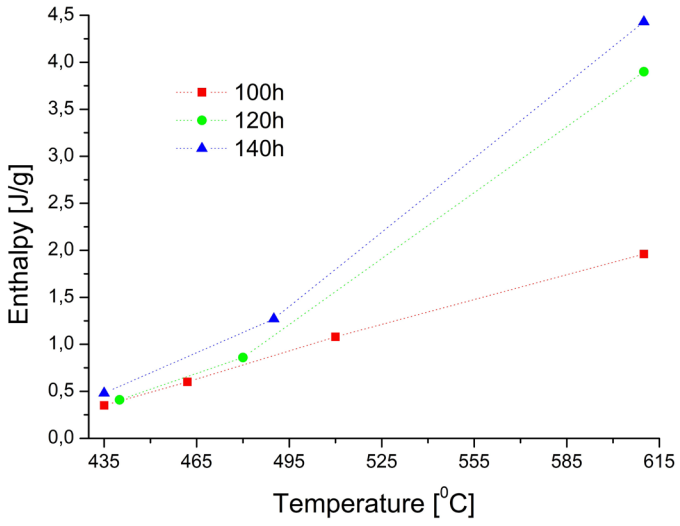

Fig. 9. Dependence of transformation enthalpy on annealing temperatures for the ground alloys

4. Summary

The comprehensive analysis of the crystallization process in the equiatomic NiTi alloy milled for: 100 h, 120 h, and 140 h, showed that it was multi-stage in the temperature range from 355°C to 558°C. The first stage was related to the crystallization of the transformable β phase, which consisted mainly of the B2 parent phase and the B19' martensite at room temperature. In addition, the non-transformable Ti_2Ni equilibrium phase crystallized at the same temperature region. In the second stage, another non-transformable Ni_3Ti equilibrium phase crystallized. According to the phase equilibrium system, this phase needed more energy to be formed.

After the third stage, the annealing temperature was relatively high and provided conditions comparable to the equilibrium one. As a result, an increase in the weight percentage of the Ti_2Ni phase was observed coming from the degradation of the β phase. Moreover, the analysis showed that extending the milling time from 100 h to 140 h decreased the crystallization temperature compared to the alloy which showed only a typically amorphous state.

Moreover, simply increasing the milling time to 140 hours improved the homogeneity of the chemical composition. It led to the formation of the areas with a chemical composition that guaranteed the occurrence of the reversible martensitic transformation. After the first stage of crystallization (annealing at

temperatures of 435-440°C), the conditions ensured the appearance of a volume capable of transforming to the martensite and returning to the parent phase with a low enthalpy – about 0.5 J/g. Enthalpy's value increased as the annealing temperature rose to almost 5 J/g, which was a much higher value than reported in the literature.

The chemical composition of the alloy, close to the equilibrium one, promoted the formation of the Ti_2Ni non-transformable phase. Hence, its amount in the alloy was visible at all stages of the thermal treatment. In addition, a titanium-based solid solution was still observed for the longer milling times of 120 h and 140 h. This fact proved another action of the colliding balls in the mill. The collisions crushed and alloyed the particles and made the previously adhered particles fall off the surface. As these particles came from the entire milling period, they contained grains with the increased Ni and Ti content. Hence, even the reported increase in the jar temperature and leaving the alloy for a long time in such conditions did not allow for the effective diffusion of alloying elements. Also, heating for a short time of 5 minutes was not enough to complete the diffusion and to homogenize the chemical composition to the level of the nominal one. The longer annealing time and/or annealing at elevated temperatures was required.

REFERENCES

[1] J. Frenzel, Z. Zhang, K. Neuking, G. Eggeler, J. Alloys Compd. **28**, 214-223 (2004).

[2] A. Foroozmehr, A. Kermanpur, F. Ashrafizadeh, Y. Kabiri, Mater. Sci. Eng. A, **528** (27), 7952-7955 (2011).

[3] J. Otubo, O.D. Rigo, C.D. Neto, P.R. Mei, Mater. Sci. Eng. A, **438**, 679-682 (2006).

[4] M. Elahinia, N.S. Moghaddam, M.T. Andani, A. Amerinatanzi, B.A. Bimber, R.F. Hamilton, Prog. Mater. Sci. **83**, 630-663 (2016).

[5] H. Kato, T. Koyari, S. Miura, K. Isonishi, M. Tokizane, Scr. Metall. Mate. **24** (12), 2335-2340 (1990).

[6] S. Green, D. Grant N. Kelly, Powder Metall. **40**, 43-47 (1997).

[7] F. Neves, F.M. Braz Fernandes, I.M. Martins, J.B. Correia, M. Oliveira, E. Gaffet, N. Boucharat, M. Lattemann, J. Suffner, H. Hahn, Mater. Sci. Forum, **636-637**, 928-933 (2010).

[8] S.L. Zhu, X.J. Yang, D.H. Fu, L.Y. Zhang, C.Y. Li, Z.D. Cui, Mater. Sci. Eng. A, **408** (1-2), 264-268 (2005).

[9] A. Biswas, Acta Mater. **53** (5), 1415-1425 (2005).

[10] B. Yuan, X.P. Zhang, C.Y. Chung, M. Zhu, Mater. Sci. Eng. A, **438-440**, 585-588 (2006).

[11] M. Bram, A. Ahmad-Khanlou, A. Heckmann, B. Fuchs, H.P. Buchkremer, D. Stöver, Mater. Sci. Eng. A, **337** (1-2), 254-263 (2002).

[12] S. Samal, O. Molnárová, F. Průša, J. Kopeček, L. Heller, P. Šittner, M. Škodová, L. Abate, I. Blanco, Appl. Sci. **11**, 1802 (2021).

[13] Y. Makifuchi, Y. Terunuma, M. Nagumo, Mater. Sci. Eng. A, **226-228**, 312-316 (1997).

[14] S.K. Sadrnezhaad, A.R. Selahi, Mater. Manuf. Processes **19** (3), 475-486 (2004).

[15] W. Maziarz, J. Dutkiewicz, J. Van Humbeeck, T. Czeppe, Mater. Sci. Eng. A, **375-377**, 844-848 (2004).

[16] H.M. Rietveld, Acta Crystallogr. **22**, 151-152 (1967).

[17] T. Goryczka, P. Salwa, Arch. Metall. Mater. **64** (3), 1017-102 (2019).

[18] T. Goryczka, P. Salwa, Metals **11**, 1908 (2021).

[19] E. Hellstern, H.J. Fecht, Z. Fu, W.L. Johnson, Mater. Res. **4**, 1292-1295 (1989).

[20] A.M. Vemula, G.C.M. Reddy, M.M. Hussain, Int. J. Mech. Eng. Technol. **8**, 398-407 (2017).

[21] T.B. Massalski, H. Okamoto, P.R. Subramanian, L. Kacprzac (Eds.), Binary Alloy Phase Diagrams, vol. 3, 2nd edn, ASM International, OH, (1990) p. 2875.

[22] G. Eggeler, J. Khalil-Allafi, S. Gollerthan, C. Somsen, W.W. Schmahl, D. Sheptyakov, Smart Mater. Struct. **14**, 186-191 (2005).

[23] W. Tang, B. Sundman, R. Sandström, C. Qiu, Acta Mater. **47** (12), 3457-3468 (1999).

[24] H. Morawiec, J. Ilczuk, D. Stróż, T. Goryczka, D. Chrobak, J. Phys. IV France **7**, C5-155 (1997).

[25] K. Madagopol, S. Banerjee, S. Lele, Acta Metall. Mater. **42**, 1875-1885 (1944).

[26] T. Goryczka, H. Morawiec, J. Alloys Compd. **367**, 137-141 (2004).